Adsorption (2014) 20:267–274
DOI 10.1007/s10450-013-9584-6

Quiescent hydrothermal synthesis of reduced graphene oxide–periodic mesoporous silica sandwich nanocomposites with perpendicular mesochannel alignments

Zheng-Ming Wang · Noriko Yoshizawa · Katsunori Kosuge · Wendong Wang · Geoffrey A. Ozin

Received: 19 May 2013 / Accepted: 30 September 2013 / Published online: 15 October 2013

Abstract Quiescent hydrothermal conditions were applied to synthesis of the sandwich nanocomposites of reduced graphite oxide (rGO) and periodic mesoporous silica (PMS) with vertically aligned mesochannels. It was found that the formation of the PMS–rGO–PMS sandwich structure is very sensitive to the surface and synthesis conditions. Although a higher temperature hydrothermal condition promotes reduction of GO and formation of bulky mesoporous nanoparticles, quiescent hydrothermal condition can serve as an alternative approach to obtain the unusual nanocomposites and slightly promote the structural stability of PMS on the surface of rGO.

Keywords Reduced graphene oxide · Periodic mesoporous silica · Sandwich · Vertical alignment · Nanocomposite

Z.-M. Wang (✉) · K. Kosuge
Adsorption and Decomposition Technology Research Group, Environmental Management Technology Research Institute, National Institute of Advanced Industrial Science and Technology, 16-1 Onogawa, Tsukuba, Ibaraki 305-8569, Japan
e-mail: zm-wang@aist.go.jp

N. Yoshizawa
Energy Storage Materials Group, Energy Technology Research Institute, National Institute of Advanced Industrial Science and Technology, 16-1 Onogawa, Tsukuba, Ibaraki 305-8569, Japan

W. Wang · G. A. Ozin
Materials Chemistry Research Group, Chemistry Department, University of Toronto, 80 St. George Street, Toronto, ON M5S 3H6, Canada

1 Introduction

In today's nanochemistry, graphene and periodic mesoporous silica (PMS) are among the most exciting classes of materials. Graphene is a single atomic layer carbon material, which exhibits excellent electrical conductivity, mechanical stiffness, thermal conductivity, and chemical reactivity (Novoselov et al. 2004; Dikin et al. 2007; Sharma et al. 2010; Allen et al. 2010). The extraordinary properties of graphene have been combined with other functionalities by forming nanocomposite structure with nanoparticles of metal and metal oxides (Wang et al. 2003; Chu et al. 2005; Stankovich et al. 2006; Compton and Nguyen 2010; Huang et al. 2012). On the other hand, PMSs have attracted interests of researchers for decades because of their high specific surface area, large pore volume, and uniform pore size, all of which allow their applications in a wide range of areas such as adsorption, catalysis, molecular sieving separation, and sensing (Kresge et al. 1992; Beck et al. 1992; Hoffmann et al. 2006). Thus it is interesting to bring together the two classes of materials to produce unexpected composite structure at nanoscopic scale.

There were already a lot of research efforts on the interfacial growth of PMS films on various types of substrates. Pioneered work by Ozin et al. have shown that PMS tends to grow at the interfaces of water and mica or water and graphite, as well as at the air and liquid interface, with their mesochannels aligned parallel to the substrate surface (Yang et al. 1996a, b, 1997; Aksay et al. 1996; Zhao et al. 1998). Subsequent researchers have strived for vertical alignment of mesochannels with respect to the substrate surface. However, these methods required expensive chemicals (special surfactants), external electrical or magnetic fields, or complex synthesis processes or setups (Koganti et al. 2006; Walcarius et al. 2007; Richman

et al. 2008). By appropriately controlling the solution chemistry of the mixtures of graphene oxide (GO), surfactants, and organic silicate sources, we have successfully obtained a novel nanocomposite structure in which thin layers of graphene oxide are sandwiched by PMS films with their mesoporous channels aligned perpendicular to the surface of carbon substrates (Wang et al. 2010).

As quiescent hydrothermal conditions are beneficial for the stable formation of PMS films on GO surface, herein we synthesize PMS–GO nanocomposite at quiescent hydrothermal conditions and compare them with those synthesized under dynamic mixing conditions. The formation of the novel nanocomposite structure was found to be very sensitive to the GO surface treatment and synthesis conditions.

2 Experimental

2.1 Materials

Graphite oxide was obtained from natural graphite by Hummers and Offeman's (1958) method and elemental analysis shows its chemical composition to be $C_8O_{4.3}H_{0.7}$ (Wang et al. 2010). GO was dispersed in dilute alkaline solution at a concentration of 0.27 mg/ml to form a solution with pH around 12. Three equal batches of these solutions were made. Batch A was sealed in a polypropylene bottle and subjected to thermal treatment at 353 K under rigorous stirring (i.e. dynamic mixing condition). Batches B and C were sealed in different reactors of Teflon-lined stainless still to allow hydrothermal treatment under quiescent condition at 353 and 373 K, respectively. The modified GOs (mGOs) made by these ways were represented as mGO-Tdm and mGO-Tq where T stands for treatment temperature and, dm and q stand for dynamic mixing and quiescent condition, respectively.

Cetyltrimethylammonium chloride (CTACl, Aldrich 25 wt% aqueous solution) was then added into mGO solution and the mixture was treated at 353 K for batch A (dm condition), and at 353 and 373 K for batches B and C (q condition), respectively, for another 1 h. Subsequently, tetraethoxysilane (TEOS) was added to each batch and hydrolysis reaction was kept for 24 h at each temperature. The amount of GO, surfactant, and TEOS used for the above synthesis were 6 mmol CTACl and 7.7 mmol TEOS per 100 g mGO solution. After hydrothermal reaction at 373 K, particles were found either to be suspended in solution or deposited at the bottom of the reactor. The two parts of particles were separated by decantation. The obtained powders were collected by centrifugation, dried at room temperature, and pyrolyzed at 773 K for 4 h in N_2 flow of 99.999 % purity. The calcined samples were the composite of reduced graphene oxide (rGO) and PMS, which were represented as rGO–PMS_353dm, rGO–PMS_353q, rGO–PMS_373qs, and rGO–PMS_373qb where s and b mean suspended and bottom parts, respectively.

2.2 Characterization

Powder X-ray diffraction (PXRD) patterns were collected on a Rigaku SmartLab-type diffractometer with a $\theta/2\theta$ Bragg–Brentano reflection geometry with fixed slits. The system is equipped with a line focus Cu Kα source operating at 40 kV and 30 mA. The scanning range was set up within the interval of $2\theta = 0.7°$–$5.0°$ with step size of 0.02° and counting time of 3.0 s per step.

UV–Vis spectra were collected on a JASCO V-650 UV–Vis spectrophotometer. GO and mGO dispersions thereafter prepared were proportionally diluted with distilled water to an appropriate absorbance range, and their absolute spectra were compared.

FT-IR spectra were measured on a Nicolet NEXUS-470 spectrometer. Water slurries of samples were dropcasted onto Si wafers, and the measurements were carried out in the 400–4,000 cm^{-1} range with a resolution of 4 cm^{-1}. A Si wafer was used as the background. The spectrometer was completely pre-purged by N_2 gas of 99.999 % purity for more than 2 h before measurement and the spectra were acquired after the complete disappearance of CO_2 signals from the tested scans.

N_2 adsorption isotherms were measured at 77 K on a BEL JAPAN Inc.-made Belsorp 18A volumetric apparatus. All the samples were evacuated at 393 K for 2 h before adsorption measurement.

The carbon contents of the composites were determined by the burnt carbon amount in a thermal gravimetric (TG) program (from 303 to 1,173 K) measured under air atmosphere and at a ramp rate of 5 K/min using a Rigaku Thermo Plus TG8120-type equipment.

Transmission electron microscopy (TEM) was carried out on a Topcon EM-002B apparatus under an accelerating electron beam voltage of 120 kV. The sample for cross-sectional observation was prepared by a standard procedure of embedding in epoxy method using Ar-milling technique.

3 Results and discussion

3.1 UV–Vis and FT-IR spectra

Figure 1 compares the absolute UV–Vis absorbance of different GO and mGO colloidal solutions. The spectrum of the as-prepared GO exhibits a main peak at 246 nm and an evident shoulder around 296 nm, which are attributed to

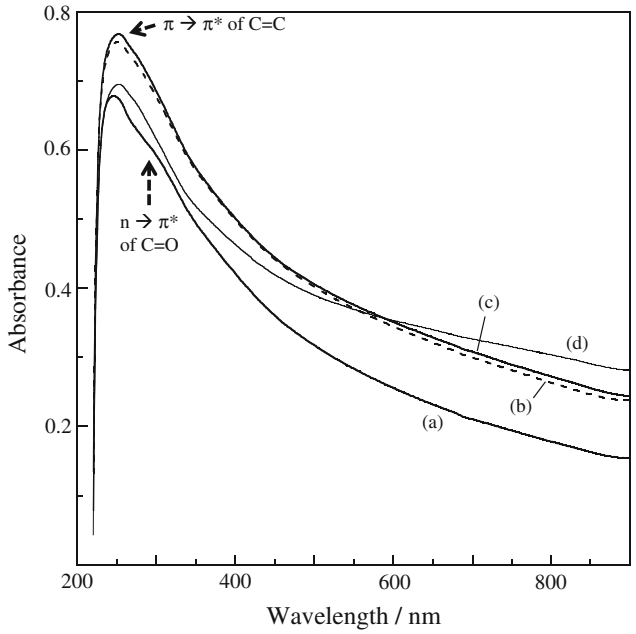

Fig. 1 UV–Vis spectra of *a* as-prepared GO, *b* mGO_353dm, *c* mGO_353q, *d* mGO_373q

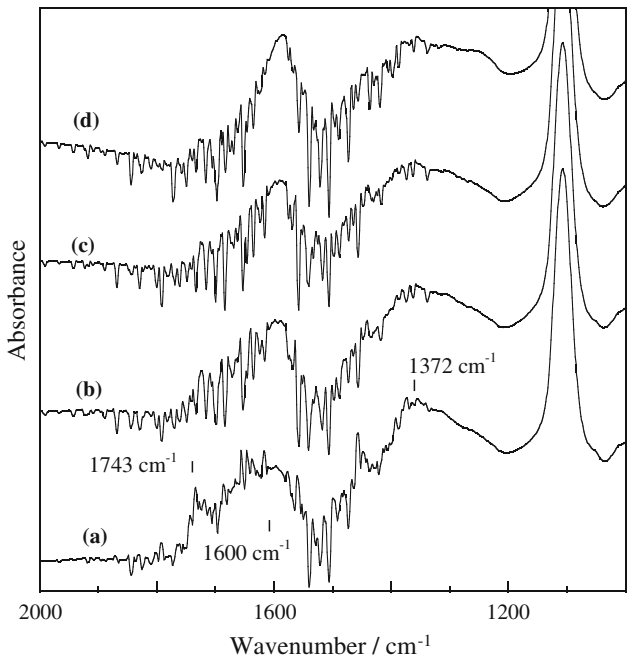

Fig. 2 FT-IR spectra of *a* as-prepared GO, *b* mGO_353dm, *c* mGO_353q, *d* mGO_373q. The 1,100 cm^{-1} peak is from the silicon substrate

the π → π* transition of aromatic –C=C– and the n → π transition of carbonyl or carboxyl –C=O groups, respectively. Through treatment under dynamic mixing, the absolute absorbance of the peak at 246 nm is apparently increased, which is accompanied by a slight red-shifting in the position of the peak (to 252 nm), a broadening in the peak shape, and a higher absorption tailing toward visible light range. This changing behavior is of the same pattern as the reported ones (Li et al. 2008; Ang et al. 2009), indicative of carbonization or partial restoration of the conjugated π structure in mGO_353dm. Disappearance of the shoulder peak around 296 nm is attributed to the loss of C=O (carbonyl or carboxyl group) on GO surface. mGO_353q displays a spectrum similar to that of mGO_353dm except for a little enhancement in absolute absorbance, demonstrating a slight promotion in aromatization of GO layers by quiescent hydrothermal treatment as compared to dynamic mixing. On the other hand, as hydrothermal temperature is increased to 373 K, the intensity of the absorption peak around 252 nm is decreased while the absorbance of the peak tailing at visible light range becomes more enhanced (Fig. 1d). The change implies that carbonization of GO layers is further proceeded and GO solution is possibly diluted due to decomposition of carbon by hydrothermal treatment at the higher temperature.

Figure 2 shows the FT-IR spectra of mGO_353q and mGO_373q in comparison with those of GO and mGO_353dm. From the spectrum of as prepared GO (Fig. 2a), evident absorption peaks can be observed at 1,743, 1,600, and 1,400–1,200 cm^{-1}, which are assigned to –C=O species of carboxyl, aromatic –C=C– species, and –C–OH species on the surface of GO, in agreement with previous results (Wang et al. 2003; Szabó et al. 2006). After treatment under dynamic mixing at 353 K, the peak at 1,743 cm^{-1} becomes ambiguous and the peak intensity at 1,600 cm^{-1} relative to that at 1,400–1,200 cm^{-1} becomes greater (Fig. 2b), indicative of the carbonization of GO by the treatment. The relative intensity of the peak at 1,600 cm^{-1} to that at 1,400–1,200 cm^{-1} further increases by quiescent hydrothermal treatment (Fig. 2c) and with the increase of treatment temperature (Fig. 2d), demonstrating the further promotion of carbonization or the restoration of π conjugation on the surface of GO. Thus, coinciding well with that of UV–Vis results, FT-IR results also display that GO surface is modified to a greater extent by quiescent hydrothermal treatment at a higher temperature as compared to dynamic mixing.

3.2 XRD and N_2 adsorption

Figure 3 shows PXRD patterns of various rGO–PMS samples. All the nanocomposites show diagnostic diffraction peaks around $2\theta = 1.7–1.9$, corresponding to *d* spacing of 4.53–5.20 nm. They are assigned to d_{100} PXRD reflections from hexagonally ordered mesopores in PMS. No second-order diffraction peaks (110 and 200 reflections) are observed in the PXRD patterns of these

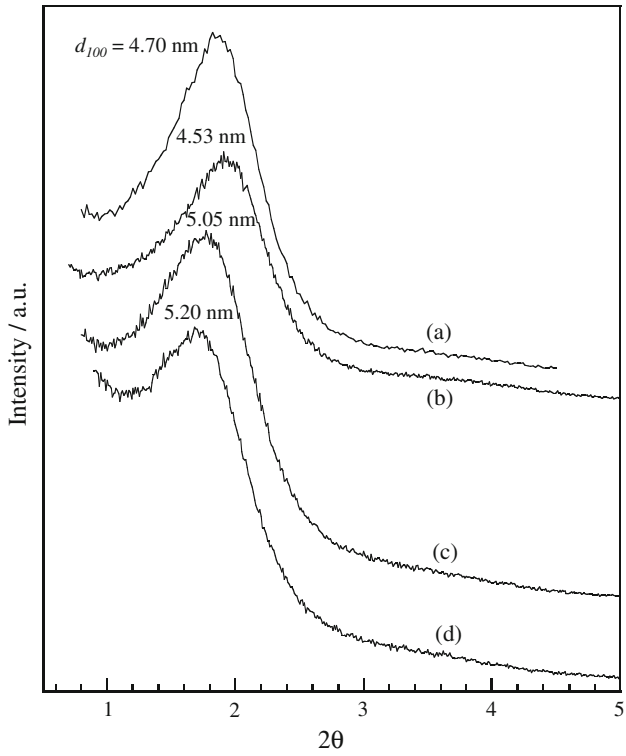

Fig. 3 XRD patterns of *a* rGO–PMS_353dm, *b* rGO–PMS_353q, *c* rGO–PMS_373qs, *d* rGO–PMS_373qb

samples, suggesting that the PMSs do not exhibit long-range order. While quiescent hydrothermal treatment leads to a little reduction in d_{100} value (from 4.70 to 4.53 nm) as compared to the dynamic mixing condition, indicative of a slight contraction of the mesoporous structure, d_{100} value changes from 4.53 to 5.20 nm through hydrothermal treatment at a higher temperature, demonstrating the expansion of mesopore array once again. The rGO–PMS_373qb sample (collected at the bottom of reactor and the sample before pyrolysis bears a blacker color) shows a weaker diffraction peak and the largest d_{100} value (5.2 nm), suggesting that the ordered mesopore structure in this sample is not as good as those in other samples.

Figure 4a shows N_2 adsorption isotherms at 77 K on the nanocomposites. The isotherm on rGO–PMS_353q exhibits a steep jump step at $p/p_0 = 0.35$–0.4 followed by a plateau area, characteristic of ordered mesopore array typical of MCM-41 materials (Gregg and Sing 1982). The jump area is more gradual as compared to MCM-41 (Kresge et al. 1992), indicative of a wider mesopore size distribution coming from the imperfect array of hexagonal geometry (Fig. 3b). The shape of the isotherm is similar to that on rGO-PMS_353dm and N_2 adsorption completely overlaps for the two samples, demonstrating that mesoporous structure in the nanocomposite is not greatly influenced by whether quiescent hydrothermal treatment or dynamic mixing condition is applied. On the other hand, porous structure is greatly changed as hydrothermal temperature is increased. While the ordered mesoporous structure-derived adsorption jumping step around $p/p_0 = 0.4$ becomes unexpectedly small, a second pore structure can be observed for rGO–PMS_373qs and rGO–PMS_373qb which are typical of a great adsorption hysteresis at $p/p_0 > 0.7$. N_2 adsorption below $p/p_0 = 0.6$ overlaps very well for the two samples but greatly deviates above $p/p_0 = 0.7$. In contrast to rGO–PMS_373qs which shows an isotherm typical of type IVa at $p/p_0 > 0.7$, rGO–PMS_373qb exhibits an isotherm closer to type IIb in this range, which is the characteristic of adsorption in aggregates of plate-like particles (Rouquerol et al. 1999). The enhanced amount of N_2 adsorption for rGO–PMS_373qs indicates a greater amount of second type of mesopores in rGO–PMS_373qs as compared to rGO–PMS_373qb.

The changing pattern of pore structure can be examined in more detail by the results of DFT pore size distributions. All samples exhibit a sharp pore size distribution centered at 4.2 nm (Fig. 4b). With increasing hydrothermal temperature, concurrently with the broadening in the 4.2 nm-centered mesopore size distribution, a second pore distribution with size ranging from 10 to 20 nm appears for rGO–PMS_373qs. Table 1 shows the pore parameters of samples, in which S_{BET} is the specific surface area calculated from the Brunauer–Emmette–Teller (BET) equation using different values of molecular sectional area (σ_{N_2}) (Gregg and Sing 1982), and S_{DFT}, $V_{0,DFT}$, and w_{DFT} are specific surface area, pore volume, and major pore size calculated by DFT methods (Thommes 2004). From these values, porosity of rGO–PMS_353q is little enhanced compared to rGO–PMS_353dm. Hydrothermal treatment at a higher temperature decreases both values of specific surface area and the 4.2 nm-centered pore volume (values in parenthesis), despite the existence of a second pore structure. The 4.2 nm-centered pores contribute to a less extent to the porosity of rGO–PMS_373qs as compared to rGO–PMS_373qb. The analysis results also confirm that the values of S_{BET} and S_{DFT} become close to each other when molecular sectional area of N_2 molecules is selected as 0.135 nm^2 rather than the usual 0.162 nm^2, which is considered appropriate for calculation of the pore structure of zeolites having polar surface.

3.3 TEM galleries of samples

Figures 5, 6 and 7 show the TEM pictures of the nanocomposites. For rGO–PMS_353q, all can be found are the plate-like morphologies in the field of vision (Fig. 5, top left). By expanding the top area of the platelets (Fig. 5, center), vertical pores coming out from the top surface of

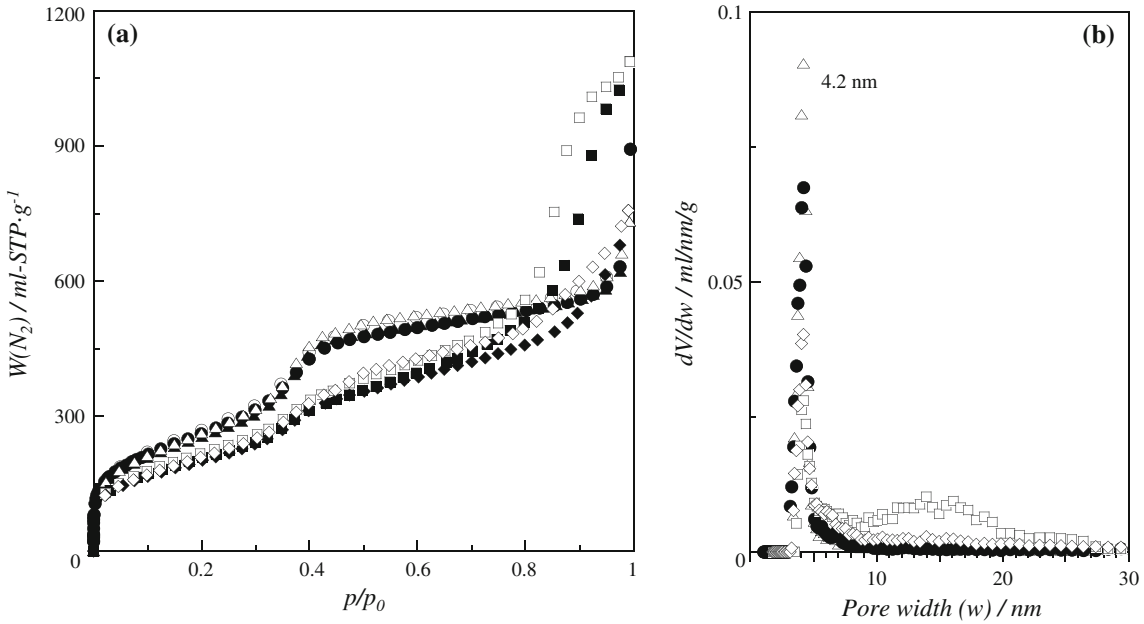

Fig. 4 **a** N_2 adsorption isotherms at 77 K on rGO–PMS_353dm (*closed circle*, *open circle*), rGO–PMS_353q (*closed triangle*, *open triangle*), rGO–PMS_373qs (*closed square*, *open square*), rGO–PMS_373qb (*closed rhombus*, *open rhombus*) where *filled* and *unfilled marks* represent the adsorption and desorption branches, respectively, and **b** their pore size distributions by DFT method

Table 1 Pore parameters of samples

Sample	S^{a}_{BET} (m^2/g)	S^{b}_{BET} (m^2/g)	S^{c}_{DFT} (m^2/g)	$V^{c}_{0,DFT}$ (ml/g)	w_{DFT} (nm)
rGO-PMS_353dm	940	785	738 (620)	0.96(0.62)	4.1
rGO-PMS_353q	931	776	745 (658)	1.01 (0.68)	4.2
rGO-PMS_373qs	768	640	664 (250)	1.60 (0.27)	4.2
rGO-PMS_373qb	735	615	600(382)	1.09 (0.40)	4.2

[a] From σ_{N_2} = 0.162 nm^2, p/p_0 range = 0.05–0.2

[b] From σ_{N_2} = 0.135 nm^2, p/p_0 range = 0.05–0.2

[c] Values in parenthesis are those of mesopores with size ranging within $w_{DFT} \pm 0.8$ (nm)

the plates are clearly visible. From some unexpected curved edge areas of the plates, one can observe some sectional areas which show deeper contrast and the presence of narrow seams in the middle (Fig. 5, right). The sandwich-type nanocomposite structure is clearly evidenced by the cross-sectional TEM picture shown in the bottom left of Fig. 5. These results disclose the formation of a nanocomposite structure very similar to that obtained by dynamic mixing in the previous report (Wang et al. 2010). Thus, quiescent hydrothermal condition is an alternative way to obtain the likewise unusual sandwich nanocomposite.

As hydrothermal temperature is further increased, it was found that a large amount of mesoporous nanoparticles of tens nanometers size was formed besides the PMS–rGO–PMS sandwich structures (Fig. 6, left). These particles either aggregate together (Fig. 6, top right) or deposited on the top surface of rGO (Fig. 6, bottom right). For rGO–PMS_373qb, one can easily observe some imperfect sandwich structure in which fragments of mesoporous parts with vertically aligned mesochannels exist on the surface of rGO (Fig. 7, left and bottom right) except for the deposited aggregates of mesoporous nanoparticles (Fig. 7, top right). Thus, the second pore structure in the two samples discussed in Fig. 4 comes from the interstitial voids between the mesoporous nanoparticles in their aggregates or between the PMS-imperfectly covered carbon platelets.

Therefore, the growth of PMS–rGO–PMS sandwich nanocomposites with perpendicular mesochannel alignment is very sensitive to the surface and synthesis conditions. By comparing dynamic mixing and hydrothermal conditions, both of which give a composite with a similar mesoporosity (mesopore size around 4.2 nm) and a similar carbon content (7.3 wt% for rGO–PMS_353dm and 6.8 wt% for rGO–PMS_353q), one can conclude that the contraction of pore wall of rGO–PMS_353q (Fig. 3) means an increased packing density of silica in pore walls due to more sufficient

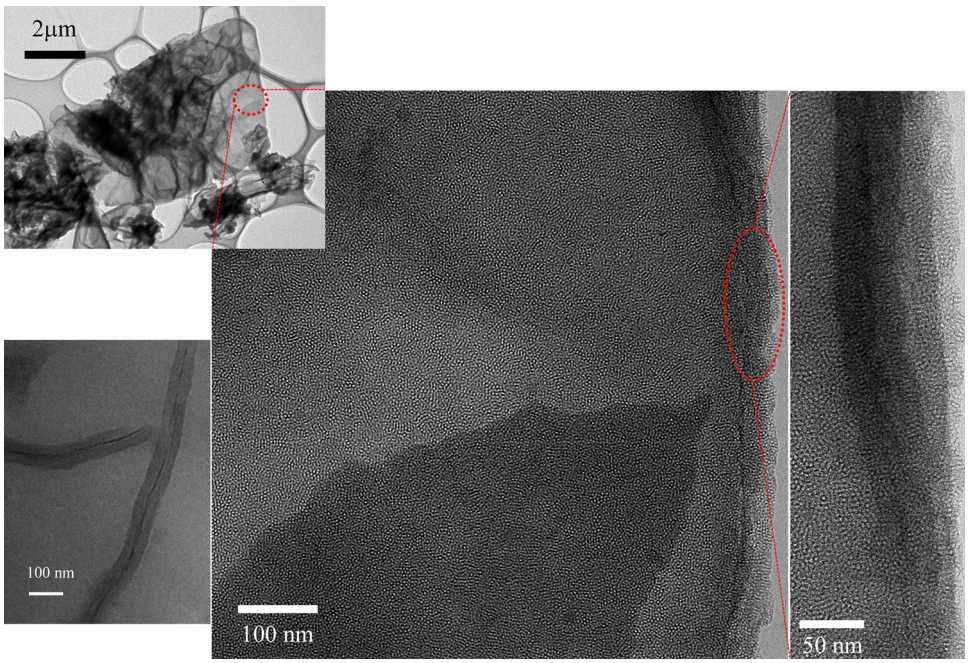

Fig. 5 TEM images of rGO–PMS_353q. The *right bottom* is the cross-sectional picture clearly showing the sandwich structure

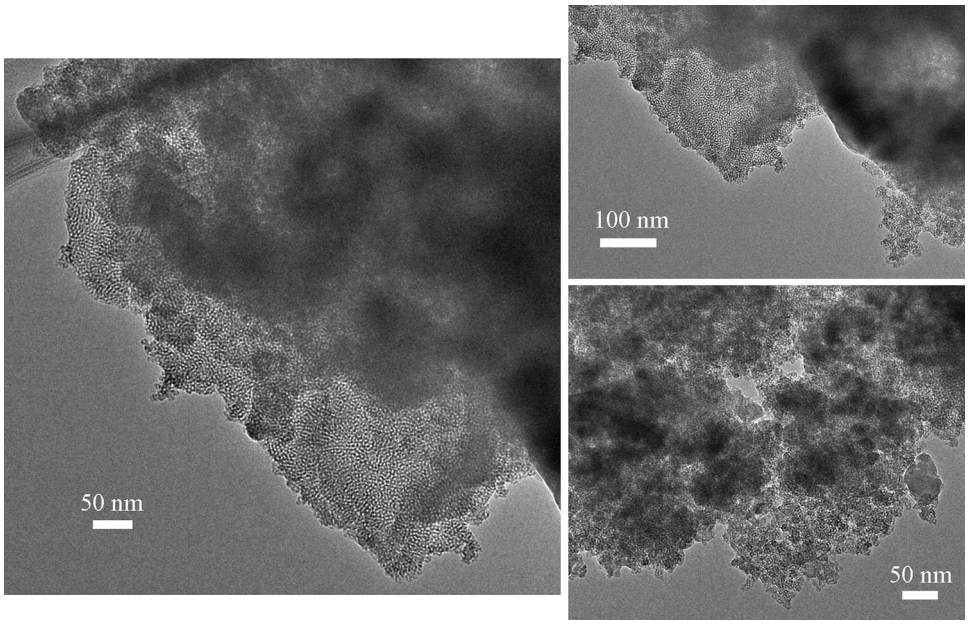

Fig. 6 TEM images of rGO–PMS_373qs

hydrolysis and polymerization reactions under hydrothermal condition. In other words, hydrothermal condition slightly promotes the formation of a more stable pore wall structure. However, higher temperature hydrothermal treatment or synthesis does not serve as a positive factor for the growth of the sandwich-type nanocomposite structure because of the modification of GO surface (the promotion of carbonization) and the acceleration of formation of nano-sized mesoporous particles in bulk solution phase. The difference between rGO–PMS_373qs and rGO–PMS_373qb is likely to be associated with the degree that carbon materials contact Si source in the course of synthesis. When experiencing a quick change in solution chemistry at a higher temperature, larger GO platelets are more easily deposited to the bottom of the reactor at a quiescent condition. This part of GO layers cannot contact Si source as sufficiently as those suspended in solution. This leads to the production of a composite in which surface of rGO is not completely covered by PMS (Fig. 7). This consideration is supported by the doubled carbon content in the resulted rGO–PMS_373qb (8.6 wt%, measureded by TG method) as compared to that in rGO–PMS_373qs (4.1 wt%), indicating that less amount of silica is composed with rGO in rGO–PMS_373qb.

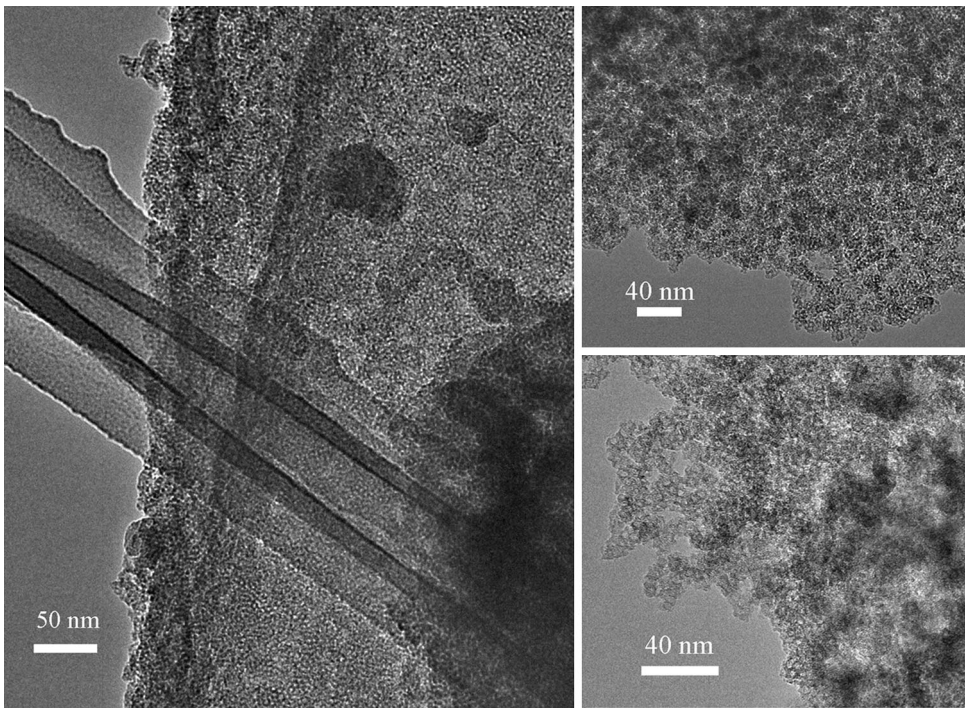

Fig. 7 TEM images of rGO–PMS_373qb

4 Conclusion

Quiescent hydrothermal conditions were applied to modify surface chemistry of GO and to synthesize the sandwich nanocomposites of rGO and PMSs with vertically aligned mesochannels and compared with those by dynamic mixing condition. UV–Vis and FT-IR results confirm that quiescent hydrothermal treatment can be an effective way for modification of GO surface although a higher temperature possibly induces the loss of one part of carbon materials. XRD, N_2 adsorption, and TEM results display that the mesopore-vertically-aligned PMS–rGO–PMS sandwich structure can be formed as perfectly by quiescent hydrothermal conditions as by dynamic mixing. Formation of PMS–rGO–PMS sandwich structure is very sensitive to surface chemistry of GO and synthesis conditions. While hydrothermal treatment at 353 K slightly increases the stability of pore walls of PMS, a higher temperature hydrothermal synthesis is not a good approach to obtain PMS–rGO–PMS sandwich structure because of easy formation of bulky mesoporous nanoparticles.

Acknowledgments This work was supported by JSPS Grants-in-Aid for Scientific Research (KAKENHI) Grant Number 24550170.

References

Aksay, I.A., Trau, M., Manne, S., Honma, I., Yao, N., Zhou, L., Fenter, P., Eisenberger, P.M., Gruner, S.M.: Biomimetic pathways for assembling inorganic thin films. Science **273**, 892–898 (1996)

Allen, M.J., Tung, V.C., Kaner, R.B.: Honeycomb carbon: a review of graphene. Chem. Rev. **110**, 132–145 (2010)

Ang, P.K., Wang, S., Bao, Q., Thong, J.T.L., Loh, K.P.: High-throughput synthesis of graphene by intercalation–exfoliation of graphite oxide and study of ionic screening in graphene transistor. ACS Nano **3**, 3587–3594 (2009)

Beck, J.S., Vartuli, J.C., Roth, W.J., Leonowicz, M.E., Kresge, C.T., Schmitt, K.D., Chu, C.T.-W., Olson, D.H., Sheppard, E.W., McCullen, S.B., Higgins, J.B., Schlenker, J.L.: A new family of mesoporous molecular sieves prepared with liquid crystal templates. J. Am. Chem. Soc. **114**, 10834–10843 (1992)

Chu, Y.-H., Wang, Z.-M., Yamagishi, M., Kanoh, H., Hirotsu, T., Zhang, Y.-X.: Synthesis of nanoporous graphite-derived carbon–silica composites by a mechanochemical intercalation approach. Langmuir **21**, 2545–2551 (2005)

Compton, O.C., Nguyen, S.T.: Graphene oxide, highly reduced graphene oxide, and graphene: versatile building blocks for carbon-based materials. Small **6**, 711–723 (2010)

Dikin, D.A., Stankovich, S., Zimney, E.J., Piner, R.D., Dommett, G.H.B., Evmenenko, G., Nguyen, S.T., Ruoff, R.S.: Preparation and characterization of graphene oxide paper. Nature **448**, 457–460 (2007)

Gregg, S.J., Sing, K.S.W.: Adsorption, Surface Area, and Porosity. Academic Press, New York (1982)

Hoffmann, F., Cornelius, M., Morell, J., Fröba, M.: Silica-based mesoporous organic–inorganic hybrid materials. Angew. Chem. Int. Ed. **45**, 3216–3251 (2006)

Huang, X., Qi, X., Boey, F., Zhang, H.: Graphene-based composites. Chem. Soc. Rev. **41**, 666–686 (2012)

Hummers, W.S., Offeman, R.E.: Preparation of graphite oxides. J. Am. Chem. Soc. **80**, 1339 (1958)

Koganti, V.R., Dunphy, D., Gowrishankar, V., McGehee, M.D., Li, X., Wang, J., Rankin, S.E.: Generalized coating route to silica and titania films with orthogonally titled cylindrical nanopore arrays. Nano Lett. **6**, 2567–2570 (2006)

Kresge, C.T., Leonowicz, M.E., Roth, W.J., Vartuli, J.C., Beck, J.S.: Ordered mesoporous molecular sieves synthesized by a liquid-crystal template mechanism. Nature **359**, 710–712 (1992)

Li, D., Müller, M.B., Gilje, S., Kaner, R.B., Wallace, G.G.: Processable aqueous dispersions of graphene nanosheets. Nat. Nanotechnol. **3**, 101–105 (2008)

Novoselov, K.S., Geim, A.K., Morozov, S.V., Jiang, D., Zhang, Y., Dubonos, S.V., Grigorieva, I.V., Firsov, A.A.: Electric field effect in atomically thin carbon films. Science **306**, 666–669 (2004)

Richman, E.K., Brezesinski, T., Tolbert, S.H.: Vertically oriented hexagonal mesoporous films formed through nanometer scale epitaxy. Nat. Mater. **7**, 712–717 (2008)

Rouquerol, F., Rouquerol, J., Sing, K.S.W.: Adsorption by Powders & Porous Solids. Academic Press, San Diego (1999)

Sharma, R., Baik, J.H., Perera, C.J., Strano, M.S.: Anomalously large reactivity of single graphene layers and edges toward electron transfer chemistries. Nano Lett. **10**, 398–405 (2010)

Stankovich, S., Dikin, D.A., Kohlhaas, K.M., Zimney, E.J., Stach, E.A., Piner, R.D., Nguyen, S.T., Ruoff, R.S.: Graphene-based composite materials. Nature **442**, 282–286 (2006)

Szabó, T., Berkesi, O., Forgo, P., Josepovits, K., Sanakis, Y., Petridis, D., Dékány, I.: Evolution of surface functional groups in a series of progressively oxidized graphite oxides. Chem. Mater. **18**, 2740–2749 (2006)

Thommes, M.: Physical adsorption characterization of ordered and amorphous mesoporous materials. In: Lu, G.Q., Zhao, X.S. (eds.) Nanoporous Materials, Science & Engineering, Chap. 11, pp. 318–364. Imperial College Press, London (2004)

Walcarius, A., Sibottier, E., Etienne, M., Ghanbaja, J.: Electrochemically assisted self-assembly of mesoporous silica thin films. Nat. Mater. **6**, 602–608 (2007)

Wang, Z.-M., Hoshinoo, K., Shishibori, K., Kanoh, H., Ooi, K.: Surfactant-mediated synthesis of a novel nanoporous carbon–silica composites. Chem. Mater. **15**, 2926–2935 (2003)

Wang, Z.-M., Wang, W., Coombs, N., Soheilnia, N., Ozin, G.A.: Graphene oxide-periodic mesoporous silica sandwich nanocomposites with vertically oriented channels. ACS Nano **4**, 7437–7450 (2010)

Yang, H., Coombs, N., Sokolov, I., Ozin, G.A.: Free-standing and oriented mesoporous silica films grown at the air–water interface. Nature **381**, 589–592 (1996a)

Yang, H., Coombs, N., Sokolov, I., Ozin, G.A.: Registered growth of mesoporous silica films on graphite. J. Mater. Chem. **7**, 1285–1290 (1997)

Yang, H., Kuperman, A., Coombs, N., Mamiche-Afara, S., Ozin, G.A.: Synthesis of oriented films of mesoporous silica on mica. Nature **379**, 703–705 (1996b)

Zhao, D., Yang, P., Melosh, N., Feng, J., Chmelka, B.F., Stucky, G.D.: Continuous mesoporous silica films with highly ordered large pore structures. Adv. Mater. **10**, 1380–1385 (1998)